

Impact of DFIG Based Offshore Wind Farms Connected Through VSC-HVDC Link on Power System Stability

Mohamed Edrah, Kwok L. Lo*, Olimpo Anaya-Lara*, Abdussalam Elansari**

**University of Strathclyde, Glasgow, UK, (e-mail: mohamed.edrah@strath.ac.uk, k.lo@strath.ac.uk, olimpo.anaya-lara@strath.ac.uk, abdussalam.elansari@strath.ac.uk)*

Keywords: DFIG, offshore wind farm, power system stability, VSC-HVDC.

Abstract

With the increased levels of offshore wind power penetration into power systems, the impact of offshore wind power on stability of power systems require more investigation. In this paper, the effects of a large scale doubly fed induction generator (DFIG) based offshore wind farm (OWF) on power system stability are examined. The OWF is connected to the main onshore grid through a voltage source converter (VSC) based high voltage direct current (HVDC) link. A large scale DFIG based OWF is connected to the New England 10-machine 39-bus test system through a VSC-HVDC. One of the synchronous generators in the test system is replaced by an OWF with an equivalent generated power. As the voltage source converter can control the active and reactive power independently, the use of the onshore side converter to control its terminal voltage is investigated. The behaviour of the test system is evaluated under both small and large grid disturbances in both cases with and without the offshore wind farm.

1 Introduction

In recent years, the integration of wind power into power systems has increased rapidly. During the last decade, the installed capacity of wind turbines has increased at an unexpected rate, and the wind turbines costs have also decreased [1]. Most of the recently installed wind turbines are variable speed wind turbines employing doubly fed induction generators. Many countries plan to build a number of large OWFs to produce a large amount of sustainable and clean energy to meet their renewable energy targets. By 2030, it is expected that about 120 GW of installed wind power in Europe will be offshore [2].

With the rapid growth of installed capacity of offshore wind power, the proportion of power generated by OWF to that generated by conventional power plants has increased. Offshore wind farms with a capacity of hundreds of MWs are large enough to replace conventional power plants. As a result, the impacts of large OWF on the power system stability will be more significant [3]. Moreover, the dynamic behaviour of VSC-HVDC transmission system during grid

disturbances is different from the well-known ac transmission systems [4].

Most of the currently installed OWFs are connected to the onshore grid by using ac transmission systems. However, with the large capacity and distance of OWFs, the ac transmission system is no longer suitable for this purpose. As OWFs are located far from onshore grids, submarine cables are the only choice to be used to transfer the generated wind power to main grids. In the case of high voltage alternating current (HVAC), which is used to be the first option, the long cables capacitance is too high leading to a large amount of capacitive current. This can reduce the cable capacity and require large reactive power compensation devices. Moreover, ac transmission systems are synchronously coupled networks, and as a result, any disturbance occurring on the onshore grid can directly affect the offshore wind farm [5-7]. Therefore, with the increase of size and distance of OWFs from the main onshore grids, a controllable power transmission system is required to connect these large OWFs to the main onshore grids. High voltage direct current (HVDC) transmission can be used as an alternative topology to traditional HVAC transmission systems. The dc link has less power losses and lower voltage drop as there is no charging current. Moreover, the offshore grid is decoupled from the onshore grid by HVDC transmission system. In this case, OWF cannot contribute to the onshore fault. In addition, VSC-HVDC can provide fast control of both active and reactive power independently [6, 8].

Although the use of VSC-HVDC within a large ac system or to connect two independent ac systems is well documented, the use of VSC-HVDC to connect a large OWF is a different case. As the use of VSC-HVDC transmission system to connect OWF is relatively new in comparison with conventional HVAC transmission system, their dynamic behaviour is still under research. The use of VSC-HVDC to connect OWF to the main grid has been reported already in some literature. In [5] the use of VSC-HVDC to link a large OWF to a weak system far from the OWF is studied. The integration OWF through HVDC light transmission system is examined by [9]. The paper concluded that the HVDC light transmission system is a promising concept to be used as a transmission system between OWF and onshore ac grid. In [10], the authors compare The dynamic performance under a fault condition of VSC-HVDC and HVAC links used to connect OWF. The paper simulation results show that the VSC-HVDC option has better fault ride through capability.

The type of OWF examined in the previous two papers is based on fixed speed induction generator. Reference [11] examined the use of VSC-HVDC and ac transmission systems to connect OWF to an onshore network. Transient capability assessments of VSC-HVDC is carried out by [12]. The transient response of the voltage source converters is examined during ac and dc side faults. Connecting remote OWF to a weak ac grid using VSC-HVDC link is examined by [5]. Simulation results demonstrated that active and reactive power can be controlled independently by using a VSC-HVDC link. This helps to keep the variation of voltage at the point of connection at an acceptable level.

This paper will examine the impacts of large DFIG based OWF (560 MW) on the power system stability. The OWF is connected to an onshore grid by VSC-HVDC link. As the voltage source converter can control active and reactive power independently, the use of the onshore side converter to control its terminal voltage is investigated. The behaviour of the test system is evaluated under both small and large grid disturbances for the cases with conventional power plant and also with OWF.

This paper is organised as follows: First, the modelling of DFIG is described in section 2. Then the modelling of VSC-HVDC is revised in section 3. Section 4 describes the test system and a number of cases. Small signal stability and transient stability analysis of the test system is discussed in section 5. Finally, the paper conclusions are summarised in section 6.

2 DFIG Modelling

The typical structure of a DFIG based wind turbine is shown in Figure 1. The DFIG consists of a wound rotor induction generator and back to back converters. Stator windings of the induction generator are connected directly to the grid while the rotor windings are connected to the grid through the back to back converter which consists of rotor side converter (RSC) and grid side converter (GSC). The power rating of the back to back converter is about 20% to 30% of the DFIG rating. With these converters, DFIG wind turbines can generate active power over a wide range of rotational speeds around the synchronous speed at constant voltage and frequency. Therefore, magnitude and direction of the active power that flows between the rotor and the grid is controlled. The induction generator is linked to the wind turbine through a mechanical shaft system consistence of high and low speed shafts connected by a gearbox. A crowbar system is used to shorten the rotor windings, in case of over current, in order to protect the converters and to achieve continuous operation of the DFIG.

The DFIG can be fully controlled by controlling both RSC and GSC as shown in Figure 2. The instantaneous active and reactive power (P_s , Q_s) of DFIG stator can be controlled independently by the RSC. Controlling the terminal voltage of DFIG can be achieved by using the stator side reactive power. The main purpose of the GSC is to maintain the dc link voltage within the limit and can be used to regulate the

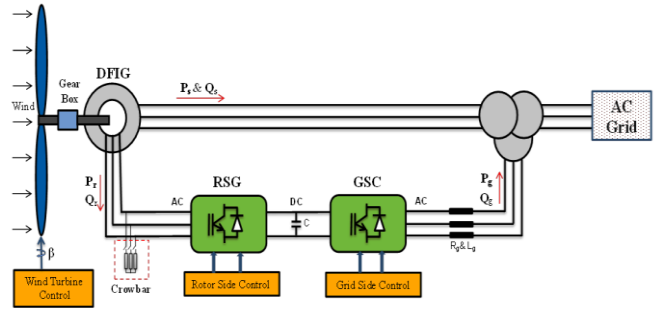


Figure 1. Typical structure of DFIG wind turbine.

reactive power exchanged between the grid and the GSC. Both converters can be modelled as current controlled voltage source converters. There are several ways to control and supply a sinusoidal current at rotor frequency. The common approach is to use pulse width modulation (PMW) [13].

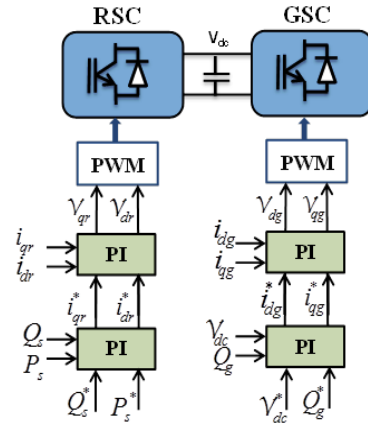


Figure 2. Overall vector control scheme of the DFIG-RSC and GSC.

Figure 2 shows the overall vector control scheme of the DFIG-RSC and GSC. The outer control loop of RSC regulates the DFIG stator active power P_s and reactive power Q_s independently. The error signals generated from comparing reference signals with measured signals of active and reactive power are passed through proportional integral (PI) controllers to generate reference signals i_{dr}^* and i_{qr}^* of the dq axes current components, respectively. These signals are compared to the measured current signals i_{dr} and i_{qr} in the dq axes to form two voltage signals by the inner control loops. These voltage signals are compensated by the corresponding cross coupling voltage in dq axes to form the dq voltage signals v_{dr} and v_{qr} , respectively. These signals are then connected to a pulse width modulation (PWM) to create signals for the IGBTs gate control.

In a similar way, the outer control loop of DFIG-GSC regulates the voltage of the dc link and the reactive power that exchanged between the grid and the GSC to generate

4 Test system

The New England 10-machine 39-bus system is adopted as a test system as shown in Figure 6 [17]. The adopted system is used to study the impact of the DFIG based OWF connected through VSC-HVDC link on power system stability. The system under study consists of 10 synchronous generators, 12 transformer, 46 transmission lines and 19 loads. Every synchronous machine is modelled in details with (TGOV1) turbine governor and (IEEEX1) exciter. In addition, generators (G_1, G_2, G_4, G_9) are equipped with (STAB1) power system stabilizer to improve the damping of low frequency oscillations in the test system. Each load is modelled as a combination of constant impedance, constant current and constant power (ZIP). The adopted system static and dynamic data can be found in [18].

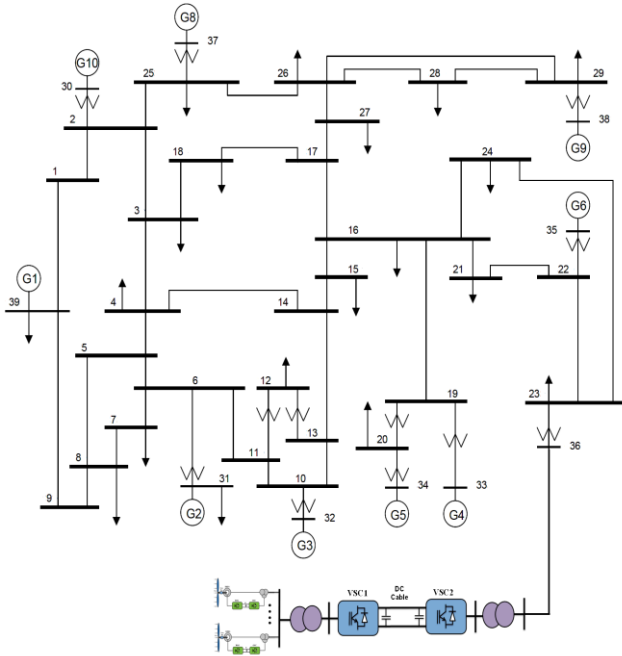


Figure 6. Single line diagram of the test system with DFIG based OWF and VSC-HVDC link.

A large scale DFIG based OWF connected to the test system through VSC-HVDC link is represented to replace the conventional synchronous generator G_7 . The OWF generated a similar amount of power to that generated by the replaced synchronous generator G_7 . The OWF consists of 112 wind turbines each rated 5 MW aggregated into a large scale DFIG wind turbine. The OWF generates 560 MW which is a similar amount to that generated by the synchronous machine G_7 . The aggregation method used to aggregate the wind turbines in this study is explained in [19]. DFIG wind turbine model includes generator model, aerodynamic model with pitch angle control, shaft model of two mass, RSC and its active and reactive power controller, GSC and its dc voltage controller and the crowbar system.

The system under study and the OWF with the VSC-HVDC link is modelled in the time domain simulation tool (NEPLAN) [20]. OWF and VSC-HVDC with their controllers are modelled as described in Sections 2 and 3.

In this study, three different cases are investigated. The description of each case is as follow:

- **Case A:** Base case scenario, all generators are conventional synchronous generators.
- **Case B:** Synchronous generator G_7 is replaced by a large DFIG based OWF with an equivalent generated power. The wind farm is connected through a VSC-HVDC link. In this case, the onshore side converter (VSC1) does not produce or absorb any reactive power.
- **Case C:** Synchronous generator G_7 is replaced by a large OWF based DFIG with equivalent generated power. The wind farm is connected through VSC-HVDC transmission. In this case, the onshore side converter (VSC1) is operating in voltage control mode (exchange the reactive power with the onshore grid) controlling its terminal voltage at 1 pu.

5 Stability analysis

5.1 Small signal stability analysis

Small signal stability of the test system is evaluated by eigenvalues analysis. Eigenvalues analysis can detect system modes, which are produced by electromechanical interactions between power system synchronous generators. Main modes with a low damping factor in the frequency range of 0.1 to 2 Hz are identified for each case.

The small signal stability results indicate that the system is stable as all eigenvalues have negative real parts. Dominant modes with low damping factor of less than 10 %, for the base case (case A), are shown in Table 1. The most critical eigenvalues are $\lambda_{1\&2}$ ($-0.218 \pm j6.611$) with damping factor of 3.3 %. Synchronous generator G_3 is the dominant machine that contributes to $\lambda_{1\&2}$ modes whereas synchronous generator G_7 is the dominant machine that contributes to the oscillatory modes $\lambda_{3\&4}$.

λ	Eigenvalue $\lambda = \sigma + j\omega$ (pu)	Damping Factor ζ (%)	Frequency (Hz)	Dominant Machine
$\lambda_{1\&2}$	$-0.218 \pm j6.611$	3.3	1.052	G_3
$\lambda_{3\&4}$	$-0.47 \pm j8.864$	5.3	1.411	G_7
$\lambda_{5\&6}$	$-0.362 \pm j6.064$	6	0.965	G_5
$\lambda_{7\&8}$	$-0.668 \pm j7.99$	8.3	1.272	G_8

Table 1: Dominant eigenvalues of case A

Eigenvalues of the study system when the synchronous generator G_7 is replaced by an equivalent OWF connected through an VSC-HVDC system (case B) are also located in the left hand side indicating a stable system. Dominant modes

with a low damping factor for case B are shown in Table 2. In this case, it is possible to note that the damping factor of $\lambda_{1\&2}$ modes have been increased from 3.3 % to 6.7 % and the damping factor of modes $\lambda_{7\&8}$ are improved slightly from 8.3 % to 8.4 %. Since the synchronous generator G_7 is replaced by the OWF, the oscillatory modes $\lambda_{3\&4}$ which are associated with generator G_7 are damped out. However, there is a new oscillatory mode $\lambda_{9\&10}$ with damping factor of 4.2 % instead of the well damped modes $\lambda_{3\&4}$ and $\lambda_{5\&6}$.

λ	Eigenvalue $\lambda = \sigma + j\omega$ (pu)	Damping Factor ζ (%)	Frequency (Hz)	Dominant Machine
$\lambda_{1\&2}$	$-0.418 \pm j6.189$	6.7	0.985	G_3
$\lambda_{7\&8}$	$-0.673 \pm j7.993$	8.4	1.272	G_8
$\lambda_{9\&10}$	$-0.28 \pm j6.719$	4.2	1.069	G_6

Table 2: Dominant eigenvalues of cases B

The results of eigenvalue analysis are demonstrated that the test system is more stable in case C when the onshore side converter controls its terminal voltage at 1 pu. This case has a lower number of low damped oscillatory modes. Moreover, modes $\lambda_{1\&2}$ and $\lambda_{7\&8}$ are damped better than the previous case as can be seen in Table 3. This is due to the reactive power used to support the system voltage.

λ	Eigenvalue $\lambda = \sigma + j\omega$ (pu)	Damping Factor ζ (%)	Frequency (Hz)	Dominant Machine
$\lambda_{1\&2}$	$-0.428 \pm j6.164$	6.9	0.981	G_3
$\lambda_{7\&8}$	$-0.682 \pm j7.995$	8.5	1.272	G_8

Table 3: Dominant eigenvalues of cases C

5.2 Transient stability analysis

To conduct transient stability analysis, a large disturbance is applied to the test system. The applied disturbance is a three-phase fault of 150 ms created near bus 16 at the transmission line connecting bus 16 and bus 24. The fault is cleared out by disconnecting the faulty line from both sides simultaneously. As the time interval of transient stability is short, wind speed during this time does not change dramatically. Therefore, in this study, the wind speed is assumed to be constant at the wind turbine rated speed.

The fault occurs at 0.5 s near bus 16 at the transmission line connecting bus 16 and bus 24. The fault is cleared out by disconnecting the faulty line at 0.65 s from both sides simultaneously. The simulation results show that the voltage at bus 36, which is the terminal voltage of G_7 and onshore side converter, is reduced to about 0.6 pu in cases A & C as shown in Figure 7a. However, it is reduced further to about 0.4 pu in case B when there is no reactive power supplied by the onshore side converter. After the fault is cleared out, the voltage recovers quickly to its initial values in cases A and C

when the terminal voltage is controlled. The voltage at bus 16, which is the nearest bus to the fault location, falls to less than 0.3 pu in the three cases as can be seen in Figure 7b. The OWF voltage is almost not affected by the disturbance in the two cases as can be seen in Figure 7c. The OWF terminal voltage remains unchanged during the fault compared to the onshore terminal voltage.

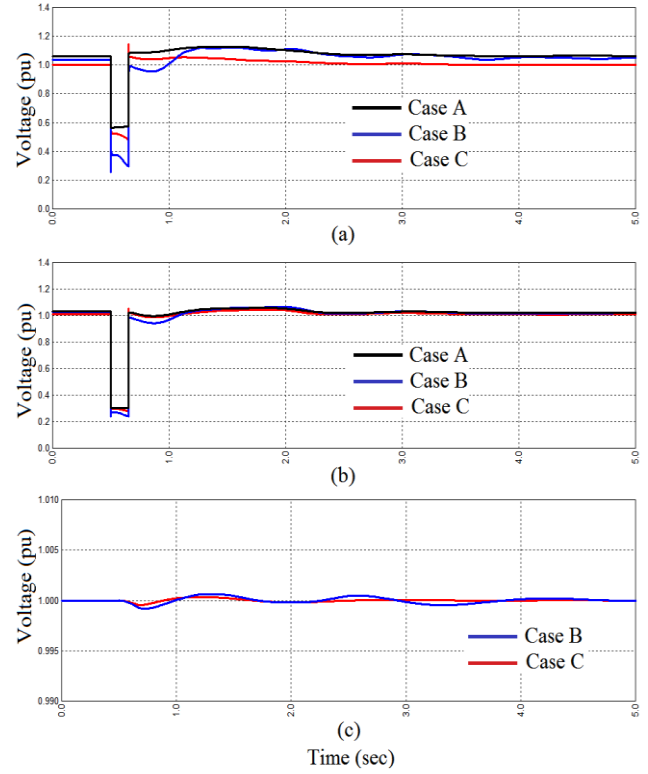


Figure 7. Transient responses of the test system voltage, (a) voltage of the critical bus 16, (b) terminal voltage of the onshore side converter and G_7 (bus 36) and (c) terminal voltage of the offshore side converter for each case.

The reactive power exchanged between the onshore side converter and the main grid is shown in Figure 8a. Prior to the disturbance, the reactive power is absorbed by the onshore side converter to maintain the terminal voltage at 1 pu when the converter controls its terminal voltage. However, prior to the disturbance, the synchronous generator G_7 is producing about 180 MVar to maintain the voltage at 1.0635 pu which is the initial value as can be seen in Figure 8a. During the fault the onshore side converter changes the sign of the reactive power to support its terminal voltage. This reactive power is controlled by the reactive power control loop of the onshore side converter. However, in case B, the reactive power that exchanged between the grid and the converter is fixed to zero. In a similar way to the offshore voltage, the reactive power exchanged between the OWF and offshore side converter is almost constant as shown in Figure 8b.

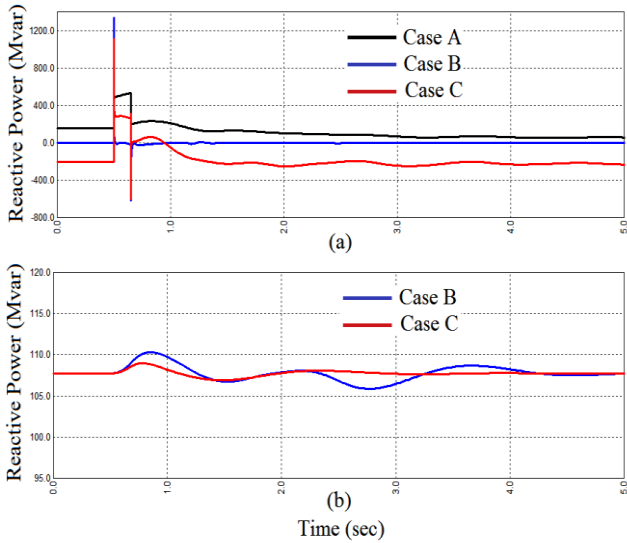


Figure 8. Reactive power of (a) onshore side converter and G_7 , (b) offshore side converter for each case.

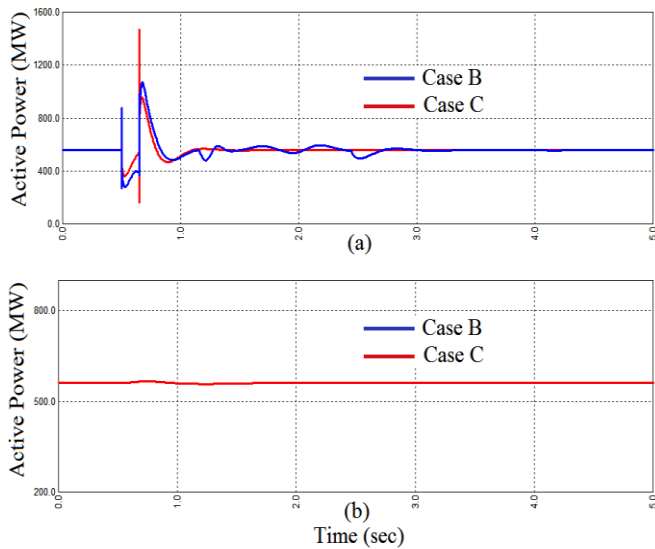


Figure 9. Active power of (a) onshore side converter, (b) offshore side converter for each case.

The transient behaviour of the active power flow during the disturbance for OWF cases is shown in Figure 9. During the fault, the active power delivered by the onshore side converter to the grid is reduced from 560 MW to about 400 MW. After the fault is removed, the active power recovers to its pre fault values within around 1 s as shown in Figure 9a. However, the active power delivered from the offshore wind farm remains stable during and after the disturbance as shown in Figure 9b. This is due to the independency between the onshore and the offshore grid decoupled by VSC-HVDC system.

6 Conclusions

In this paper, the impact of the DFIG based offshore wind connected through VSC-HVDC link on small signal and transient stability was examined for a large system. The small signal stability of the test system was evaluated by eigenvalues analyses. From the results of the eigenvalue analysis, it can be concluded that the system has less critical electromechanical oscillatory modes with OWF connected to the onshore grid through VSC-HVDC.

The time domain simulation results of a three-phase fault of 150 ms on the onshore grid show that the stability of onshore grid is degraded to some extent when the conventional synchronous generator is replaced by equivalent OWF and HVDC system. However, with the ability of the voltage source converter of the HVDC system to control active and reactive power independently, the power system stability can be enhanced by controlling the reactive power of the onshore side converter to support its terminal voltage. In the case of voltage control mode, the voltage and power after the fault recover quickly with less fluctuation. The dynamic simulation results also show that onshore grid fault cannot influence OWF behind HVDC transmission system. Due to the technical advantages the VSC-HVDC technology, the OWF is well protected against the onshore grid faults.

References

- [1] T. Ackermann, *Wind Power in Power Systems*: John Wiley & Sons, Ltd, 2005.
- [2] S. K. Chaudhary, R. Teodorescu, and P. Rodriguez, "Wind Farm Grid Integration Using VSC Based HVDC Transmission - An Overview," in *Energy 2030 Conference, 2008. ENERGY 2008. IEEE*, 2008, pp. 1-7.
- [3] C. Chompoo-inwai, L. Wei-Jen, P. Fuangfoo, M. Williams, and J. R. Liao, "System impact study for the interconnection of wind generation and utility system," *Industry Applications, IEEE Transactions on*, vol. 41, pp. 163-168, 2005.
- [4] G. O. Kalcon, G. P. Adam, O. Anaya-Lara, S. Lo, and K. Uhlen, "Small-Signal Stability Analysis of Multi-Terminal VSC-Based DC Transmission Systems," *Power Systems, IEEE Transactions on*, vol. 27, pp. 1818-1830, 2012.
- [5] X. I. Koutiva, T. D. Vrionis, N. A. Vovos, and G. B. Giannakopoulos, "Optimal integration of an offshore wind farm to a weak AC grid," *Power Delivery, IEEE Transactions on*, vol. 21, pp. 987-994, 2006.
- [6] R. Sharma, T. W. Rasmussen, K. H. Jensen, and V. Akhmatov, "HVDC Solution for Offshore Wind Park Comprising Turbines Equipped with Full-Range Converters," in *Scientific proceedings-EWEC conference and exhibition*, 2010, pp. 171-173.
- [7] S. Cole and R. Belmans, "Transmission of bulk power," *Industrial Electronics Magazine, IEEE*, vol. 3, pp. 19-24, 2009.

- [8] P. Bresesti, W. L. Kling, R. L. Hendriks, and R. Vailati, "HVDC Connection of Offshore Wind Farms to the Transmission System," *Energy Conversion, IEEE Transactions on*, vol. 22, pp. 37-43, 2007.
- [9] A.-K. Skytt, P. Holmberg, and L.-E. Juhlin, "HVDC Light for connection of wind farms," in *Second International Workshop on Transmission Networks for Offshore Wind Farms Royal Institute of Technology Stockholm, Sweden*, 2001.
- [10] A. Reidy and R. Watson, "Comparison of VSC based HVDC and HVAC interconnections to a large offshore wind farm," in *Power Engineering Society General Meeting, 2005. IEEE*, 2005, pp. 1-8 Vol. 1.
- [11] G. Ramtharan, A. Arulampalam, J. B. Ekanayake, F. M. Hughes, and N. Jenkins, "Fault ride through of fully rated converter wind turbines with AC and DC transmission," *Renewable Power Generation, IET*, vol. 3, pp. 426-438, 2009.
- [12] G. P. Adam, S. J. Finney, K. Bell, and B. W. Williams, "Transient capability assessments of HVDC voltage source converters," in *Power and Energy Conference at Illinois (PECI), 2012 IEEE*, 2012, pp. 1-8.
- [13] R. Pena, J. C. Clare, and G. M. Asher, "Doubly fed induction generator using back-to-back PWM converters and its application to variable-speed wind-energy generation," *Electric Power Applications, IEE Proceedings -*, vol. 143, pp. 231-241, 1996.
- [14] Q. Wei, G. K. Venayagamoorthy, and R. G. Harley, "Real-Time Implementation of a STATCOM on a Wind Farm Equipped With Doubly Fed Induction Generators," *Industry Applications, IEEE Transactions on*, vol. 45, pp. 98-107, 2009.
- [15] L. Qu and W. Qiao, "Constant power control of DFIG wind turbines with supercapacitor energy storage," *Industry Applications, IEEE Transactions on*, vol. 47, pp. 359-367, 2011.
- [16] S. Ruihua, Z. Chao, L. Ruomei, and X. Zhou, "VSCs based HVDC and its control strategy," in *Transmission and Distribution Conference and Exhibition: Asia and Pacific, 2005 IEEE/PES*, 2005, pp. 1-6.
- [17] T. Athay, R. Podmore, and S. Virmani, "A Practical Method for the Direct Analysis of Transient Stability," *Power Apparatus and Systems, IEEE Transactions on*, vol. PAS-98, pp. 573-584, 1979.
- [18] M. A. Pai, *Computer techniques in power system analysis*: Tata McGraw-Hill Publishing Company, 1979.
- [19] M. Pýller and S. Achilles, "Aggregated wind park models for analyzing power system dynamics," 2003.
- [20] B. B. C. P. Inc. "NEPLAN® Power System Analysis and Engineering", Available: http://www.neplan.ch/html/e/e_home.htm